Electrical Discharge Machining of Austempered Ductile Iron

Uma Batra
Department of Materials and Metallurgical Engg.,
PEC University of Engineering and Technology, Chandigarh, India
E-mail: umabatra2@yahoo.com

Abstract—*The present work investigated the effect of three machining parameters peak current (Ip), pulse on-time (Pon) and pulse off-time (Poff) on the material removal rate (MRR) and surface roughness (SR) on electric discharge machining of three ADIs. The characteristics of the surface modification layer on the ADIs were also investigated. Experimental work was conducted on three ADIs with copper electrode as tool electrode with kerosene oil as dielectric fluid. L 9 orthogonal array of Taguchi experimental design was used to conduct the experiments. The data compiled during experimentation has been analysed using two way Anova to study the effect of machining parameters on MRR and SR. Detail analysis of structural features of EDMed surfaces was done by using SEM and XRD. The same set of peak current (Ip), pulse on-time (Pon) and pulse off-time (Poff) result in the best MRR and SR. Experimental results indicated that the EDMed surface shows a continuous ridge appearance and the ridge density is closely related to the density of graphite particles. The structural analysis showed that the rapidly solidified layer comprises mainly of γ Fe, metastable phase martensite and carbides.*

Keywords: *Electric Discharge Machining, Anova, Rapidly Solidified Layer, Austemepered Ductile Iron*

INTRODUCTION

Austempered Ductile Iron (ADI) has great potential to improve the design of the components of ductile cast iron and substitute steel parts due to the exceptional combination of mechanical properties equivalent to cast and forged steels and production costs similar to those of conventional ductile iron. Although initially hindered by lack of information on properties and successful applications, ADI has become an alternative industrial material for design and construction of the components in many applications that were previously the exclusive domain of steel castings, forgings, weldments, powdered metals and aluminum forgings and castings [1, 2]. ADI is not as easily machined as regular ductile iron and this creates a major challenge in machining by conventional machining methods. Many investigations have adopted– such a tool life, tool wear rate, cutting forces, and surface finish produced a job as general criteria for evaluating the machining methods of ADI [3–8]. The improved method of machining ADI materials is now considered as one of the most important aspects of the manufacturing industries. Since, it is difficult to find tool material, which is sufficiently hard and strong to cut austempered ductile iron. In addition manufacturing of complex shapes with better surface finish, precise tolerance and higher production rates of ADIs by traditional methods is even more difficult. Therefore, non traditional machining technique likes electron discharge machining (EDM) can be considered because there is no direct contact between electrode and work piece, and material of any hardness, strength can be easily cut out with required complex shapes, better surface finish and accuracy.

Material removal of Ductile Iron using electro-discharge machining (EDM) method has been considered by some researchers [9, 10]. They have reported that a resolidified surface layer of high hardness forms close to the EDMed surface. The thickness of the resolidified layer depends on carbon content of the ductile iron and the roughness of EDMed surface depends on the graphite area fraction and graphite particle size. In fact, increasing carbon content leads to numerous discharging points. Since silicon content of ductile iron influences considerably the graphite particle size, it affects the surface roughness. Thus combined effect of carbon and silicon on surface roughness of EDMed surface of ductile iron can also be expressed as a function of carbon equivalent. Previous studies have also reported the structure of EDMed surface layers in ferrous alloys [11–13]. Austenite-martensite or austenite-ledeburite structures have been reported in plain carbon steels and low alloy steels. Martensite, ferrite, glassy phase and metastable carbides were observed in die steels [11]. The resolidified layer in Fe-C-Si alloys consisted of austenite and ε-carbide as observed in rapidly solidified Fe-C-Si alloys by splat cooled method or rotating water atomization process.

The present work investigates the electric discharge machining of three ADIs using copper electrode. L 9 orthogonal array of Taguchi experimental design was used to conduct the experiments. Three levels of three machining parameters, namely: peak current (I_p), pulse on-time (P_{on}) and pulse off-time (P_{off}) constituted the array. Negative polarity of the tool electrode and kerosene dielectric with side flushing was used for all experiments. Increase in material removal rate and surface finish were taken as performance indicators of good machining of ADIs.

EXPERIMENTAL PROCEDURES

A ductile iron of composition 3.48 C, 2.028 Si, 0.22 Mn, 0.05 Cr, 0.016 Ni, 0.6 Cu, 0.04 Mg, 0.04 Ti, 0.03 Mo, 0.0079 Sn, 0.012V, 0.02 Al, balance Fe (wt%) was produced in a commercial foundry using an induction melting furnace of medium high frequency. While high manganese ductile iron can be easily produced, the production of low manganese ductile iron is extremely difficult from practical point of view therefore, in present work, a commercially viable ductile iron with minimum

possible manganese content was produced. Copper was chosen to compensate for reduction in austemperability due to lowering of manganese content. Copper in contrast to manganese does not segregate at cell boundaries and therefore supports uniformity in austempered structure. The molten metal was poured from about 1420°C in a ladle preheated to 800°C for sandwich treatment by spheroidization technique using Fe-Si-Mg alloy (5 to 7% Mg) for nodulizing and FeSi (Si 65%) for inoculation. Post inoculation was performed with FeSi (Si 65%). The molten metal was cast immediately in the shape of modified 2.5 cm (1 in) Y-blocks. The qualitative and quantitative analysis of microstructure of the as-cast ductile iron was observed under optical microscope (Carl Zeiss) using Image analyzer (Mutech). The microstructure of as cast ductile iron is shown in Fig. 1 and the structural parameters are presented Table 1. The tensile test and wear test samples were machined from the leg part of the Y-block castings in accordance with ASTM specifications A 536-80 [14]. These samples were austenitized at 900°C for 60 minutes and transferred rapidly to a salt bath held at preselected austempering temperature (270°C, 330°C or 380°C) before quenching in water. The samples austempered at 270°C, 330°C and 380°C were designated as ADI-1, ADI-2, ADI-3 respectively. Metallographic examination of ADI samples was carried out using scanning electron microscopy (SEM, JEOL 840A). X-ray diffraction analysis (XRD, PW 1148/89) was performed on ADI samples using Cu Kα radiation (λ=1.54Å) at 40KV and 20mA in 2□ range 40° to 93°, step size 0.1°, with count time of 2 seconds per step. The averages of volume fraction of austenite, X_γ, average carbon content of high carbon austenite, C_γ, and the effective "particle size" d_α, ferrite in ausferrite product were estimated from XRD patterns of ADI-1, ADI-2, and ADI-3 following procedure described by Cullity [15].

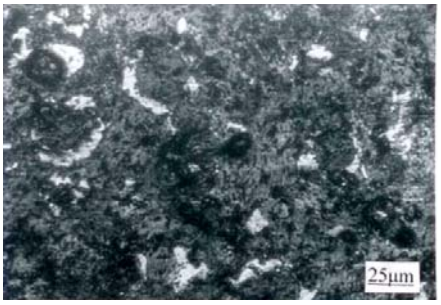

Fig. 1: Microstructure of Cast Ductile Iron

Table 1: Structural Parameters of Cast Ductile Iron

Area Fraction of Graphite Nodule, Ag (%)	Average Diameter of Graphite Nodule, dg (mm)	Number of Graphite Nodules per mm2, Ng
11.2	0.02	250

Hardness of all ADI samples was determined using Vicker's Hardness Tester (IE make) with 10 Kg load. Tensile tests were performed for each ADI on universal tensile testing machine of capacity 20 tons, UTS-20 (FI make) to estimate ultimate tensile strength (UTS), 0.2% proof stress ($\sigma_{0.2}$), and percent elongation (% El). Machining of ADI samples was carried out on Electrical Discharge Machine with conventional copper tool electrode. Time for each machining cut was fixed at 10 min. The input machining parameters and their levels used for experimentation are given in Table 2. The equipment used in EDM experiment is illustrated in Fig. 2 and Table 1 displays the settled experimental parameters. The state of discharged craters on the EDMed surface was indicated by ridge density, which was detected by surface roughness meter. The ridge is defined as the peak on the surface which is higher than the average roughness value (Ra). Surface roughness was measured using surface roughness tester Mitutoyo SJ20 with traversing length of 2–5 mm and profile resolution of 12nm. Material removal rate was determined using following equation:

MRR = Diff. in weight of work piece before and after machining/ Time of machining

The weight measurement was done using Denver make Precision Analytical Balance with an accuracy of 0.001 gm. Surface morphology and the resolidified layer were observed by SEM. XRD was used to analyze the phases present in the resolidified layer. All scans were done in steps of 0.1° interval of 2□ with count time of 2 seconds per point in the range from 0° to 90°.

Table 2: Machining Parameters used for the Experimentation

Sparking voltage	135±5V
Peak Current	4, 6, 8 A
Pulse on-time	15, 30, 45 μS
Pulse off-time	5, 7, 9 μS
Servo Control	Electro Mechanical
Polarity	Reverse (Electrode negative)
Dielectric fluid	Commercial grade Kerosene
Machining time	10 min for each cut
Electrode (+)	Electrolytic copper
Specimen (-)	ADI1, ADI2, ADI3
Fluid pressure kg/mm2	0.7
Duty factor*	0.5

*Duty factor is the ratio of pulse duration to a total pulse period.

RESULTS AND DISCUSSION

Microstructure

The SEM micrographs of ADI-1, ADI-2, and ADI-3 are shown in Fig. 2. Three ADIs exhibit unique microstructure of ausferrite comprising of acicular ferrite and high carbon austenite. Fig. 2a shows microstructure of ADI-1 in which extremely fine ferrite plates are separated by thin films of high carbon austenite. In ADI-2, ferrite plates have grown in length as well as width (Fig. 2b). ADI-3 consists of more equiaxed blocks of austenite between non parallel "sheaves" of ferrite platelets (Fig. 2c).

Structural Parameters

The X_γ, C_γ, and d_α estimated from XRD patterns of ADI-1, ADI-2, and ADI-3 are presented in Table 2. It is evident that d_α and X_γ increase appreciably with rise in austempering temperature from 270°C to 380°C, and it is in agreement with the trend reported earlier [16, 17]. The average C_γ in ADI-1, ADI-2, and ADI-3 were estimated to be 1.65, 1.77 and 1.8 (wt.%), respectively. As reported earlier, that the carbon content in austenite after water quenching of DI from 900°C was 0.85 wt.% [18]. It can be seen in Fig. 3a that the austenite matrix has martensitic start temperature much below room temperature, thus austenite formed during austempering is stabilized and does not transform to martensite on cooling to room temperature. A fully transformed ADI would have an austenite carbon content at metastable $(\alpha+\gamma)/\gamma$ phase boundary shown in Fig. 3a [19]. A preliminary investigation carried out by authors to find out the austempering time required to produce fully transformed ADI at 380°C and 320°C. In fully transformed ADIs at 380°C for 60 minutes and 320°C for 120 minutes, the average carbon contents were found to be 1.8 wt.%, and 1.9 wt.% respectively [20]. These data two points were used to project carbon content of metastable boundary at 270°C of approximately 2.0 wt.%. Comparing these with actual C_γ in ADI-1, ADI-2 and ADI-3 (Table 2), it becomes evident that carbon content in austenite did not reach the projected phase boundary in ADI-1 and ADI-2, implying that the transformation had not been completed at 320°C and 270°C for 1 hour (Fig. 3b). The average carbon content in ADI-1 is about 83 % of the projected phase boundary carbon content as compared to nearly 94% and 100% in ADI-2 and ADI-3, respectively. It is reasonable to assume that the intercellular region in ADI-1 contains some martensite due to insufficient carbon enrichment of austenite in last to transform region. This is in contrast to SEM micrograph where the matrix appeared to be completely transformed into very fine ausferrite structure.

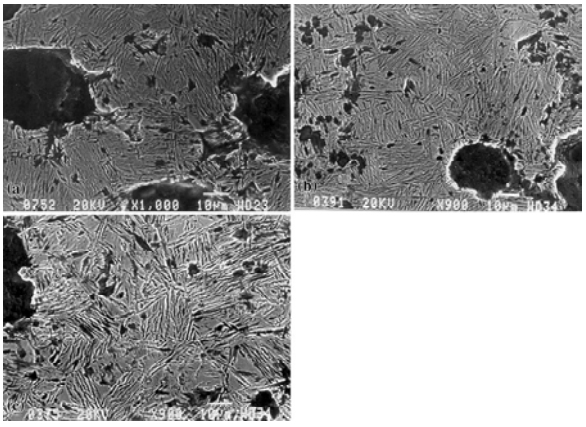

Fig. 2: SEM Images of (a) ADI-1, (b) ADI-2, and (c) ADI-3

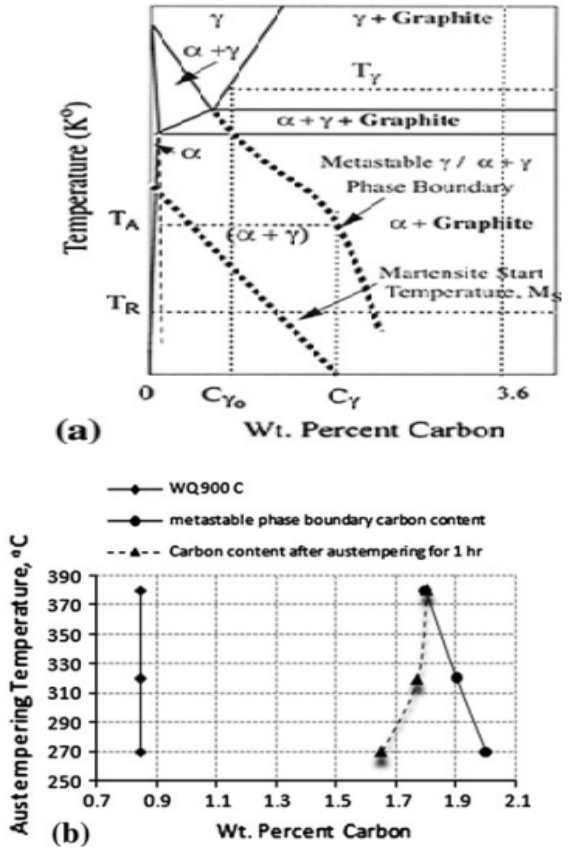

Fig. 3: (a) Schematic Fe-C-Si Diagram [24] and (b) Phase Boundary for $(\alpha+\gamma)/\gamma$ Determined by XRD

Mechanical Properties

The mechanical properties of the ADI-1, ADI-2, and ADI-3 are given in Table 2.

Table 2: Structural Parameters and Mechanical Properties of ADI-1, ADI-2, and ADI-3

ADI	Xγ	Cγ, (wt.%)	dα (Å)	Hardness HV10	UTS MPa	σ0., MPa	% El
ADI-1	0.26	1.65	162	445	1340	1276	3.7
ADI-2	0.36	1.77	190	354	1094	881	10.2
ADI-3	0.43	1.95	252	327	887	701	8.5

ADI-1 show maximum values for hardness, UTS, and $\sigma_{0.2}$, but minimum value for % El, which is apparently due to sluggish ausferrite kinetics at 270°C, resulting in incomplete ausferrite transformation and intercellular regions containing some martensite. With increase in austempering temperature from 270°C to 380°C, hardness, UTS, and $\sigma_{0.2}$ of ADI decrease in accordance with coarsening of the ausferrite, and %El improves due to increased amount of austenite phase in the matrix [18]. Strain hardening exponent, n, was found to rise steadily with rise in austempering temperature (Table 2). Mechanical properties depend upon the stability of the

austenite during deformation. Parameters like carbon content of the austenite, size and morphology of austenite, and its distribution within the microstructure control the stability of austenite [21–24]. The chemical driving force for the transformation of austenite to martensite is determined by the carbon content. Austenite containing less than 0.6 wt.% carbon is known to transform rapidly to martensite during deformation. In the present work, the average carbon contents of austenite in ADIs are in the range of 1.6 to 2.0 wt.%, thus it can be ruled out as an important parameter. Thin films of austenite are more stable than blocky austenite, as they contain less potential sites for nucleation of martensite [25, 26]. Therefore, austenite in ADI-1 and ADI-2 is presumed to be relatively more stable than in ADI-3. Besides this, blocky austenite areas between the ferrite sheaves will be enriched with carbon by diffusion over longer diffusion distance, and if the carbon does not diffuse up to center, it tends to transform to martensite during quenching. The phase present in the vicinity of the austenite is an added important factor. If martensite is present in the vicinity of austenite, the latter can transform to martensite during early stages of straining, whereas, ferrite present in its neighborhood can act as a barrier to autocatalytic propagation. Therefore, on account of size, morphology, and distribution of austenite in ADI microstructure, the strain induced transformation of austenite is more likely in ADI-3 as compared to ADI-1 and ADI-2.

Surface Roughness and Material Removal Rate

All the machined surfaces thus obtained were subjected to micro hardness using a load of 9.807 N for a dwell time of 20 S. Surface roughness testing material removal rates were calculated under different machining conditions. This data was analyzed to find out the desirable combination of levels of three input process parameters, their significance and relative contribution. The best achieved surface finish and material removal rate after machining for each work material are given in Table 4. Samples showing best surface finish and material removal rate were further subjected to:

X-ray diffraction (XRD) analysis to find out the phases present, Scanning electron microscopy to analyze the structural features of the machined surfaces, Composition testing on spectrometer to analyze material transfer and quantitative analysis of the changes in the constituents of the machined surfaces.

Table 4: Surface Roughness and Material Removal Rates of Three ADIs after Machining

ADIs	Surface Roughness Avg. Ra (μm)	MRR (gm/min)
ADI-1	2.09	0.36
ADI-2	2.223	0.29
ADI-3	2.021	0.37

The upper material in extremely high temperature region vaporizes, while the lower material melts. Two regions are clearly visible-one is original material and another is recast layer, which has a brighter white colour.

A smaller thermal gradient occurs at the lower pulse current, thus forming a thinner recast layer. The recast layer appears thick as the pulse current increase because at higher pulse current, a steeper thermal gradient builds up possibly causing a thermal effect beneath the melting zone. This phenomena leads to a greater removal of molten layer that is not flushed out by the dielectric fluid but it re-solidifies and remain attached to the mechanical surface. The thickness of recast layer depends on electrode material type of dielectric and also flushing condition. EDM erodes the surface randomly and the surface finish is poor because of more frequent cracking of dielectric fluid as well as metal expulsion.

Optimum Machining Parameters

The optimum machining parameters for three work piece and the relative contribution of the factor have been summarized in Table 5, it is found that the contribution of input machining parameters for the best surface finish is same for all the three ADIS. Even the relative contribution of the factor is almost identical. Hence, it can be conclusively inferred from this data that the input process parameters are independent of type of ADI and same value will hold good for any ADI. Peak current emerges as the most significant factor with more than 20% contribution in all cases. Another important observation is that the contribution of pulse-on time is more than pulse-off time. It means pulse-on time is more significant and sufficient time is essential for the work piece to undergo melting or evaporation in response to sparking.

Features of Edmed Surface

Figure 4 shows the representative resolidified layer formed in the vicinity of the EDMed surface of specimens. The morphology of EDMed surface is illustrated in Fig. 5, showing a wavy ridge pattern formed by overlapping craters. The clustered graphite particles were found to be located in the troughs in-between the ridges. Fig. 5 indicates that the ridge density tends to increase with rise in austempering temperature. The compositional analysis of resolidified layer shows that resolidified layer has compositions similar to that of the base material, which indicates that the element of the electrode (Cu) does not transfer on the resolidified layer. Fig. 6 displays the X-ray diffraction pattern and the EDMed surface of ADI-1, ADI-2, and ADI-3 specimens. The austenite, martensite and carbide phases have been identified.

Table 5: Optimum Process Parameter and their Relative Contribution for the Best Value of Surface Roughness

Parameter	For Best Surface Finish			For Maximum MRR		
Work Materials	ADI-1	ADI-2	ADI-3	ADI-1	ADI-2	ADI-3
Optimum setting	$A_3 B_3C_3$	$A_3 B_3C_3$	$A_3 B_3C_3$	$A_3 B_2C_1$	$A_3 B_2C_1$	$A_3 B_2C_1$
Peak current contribution	85.21	91.10	89.17	89.41	76.22	81.74
Pulse on time contribution	11.05	5.50	6.31	7.86	19.58	14.18
Pulse off time contribution	1.71	3.05	1.84	0.92	2.70	0.93

Factor A: Represents peak current and level A_1 = 4A, A_2 = 6A, A_3 = 8A

Factor B: Represents peak on time and level B_1, = 15µs, B_2 = 30µs, B_3 = 45µs

Factor C: Represents peak off time and level C_1, = 5µs, C_2 = 7µs, C_3 = 9µs

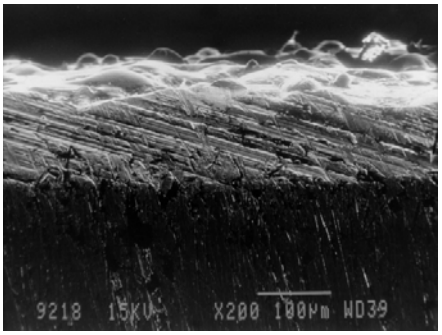

Fig. 4: Resolidified Layer after EDM Operation of ADI

DISCUSSION

The EDM process is carried in a dielectric fluid, with a small gap between the work piece and the electrode. The bulgy area could be considered causing a strong likelihood for discharge to occur. Since the temperature at the discharge point is expected to be exceeding 3000°C, rapid melting and evaporation occur on portions of the surface including graphite and ausferrite regains. Only a small portion of the melt produced by the discharge, about 15% is carried away by the dielectric [27]. The remaining melt rapidly solidifies and forms a layer with an undulant surface. The following dielectric plays an important role in heat sinking during rapid solidification. Thus, the variations in hardness along the through thickness direction of this rapidly solidified layer can be inferred to be the cooling rate gradient. With each discharge, a crater is formed on the work piece due to discharge, impact generated during EDM [28]. The EDM process is ADI is illustrated schematically in Fig. 7. At the first stage, the sparks and the melting occurs successively (Fig. 7 (a)), and then residual melt solidifies. Considering the poor wet ability between the melt and graphite [29] the graphite particles are dewetting from the molten material and thus the semi-matter graphite will be situated on the cavities of the EDMed surfaces (Fig. 7(b)). The ridge formed between the semi molten graphite can be considered to the next sparking position (Fig. 7(c)).

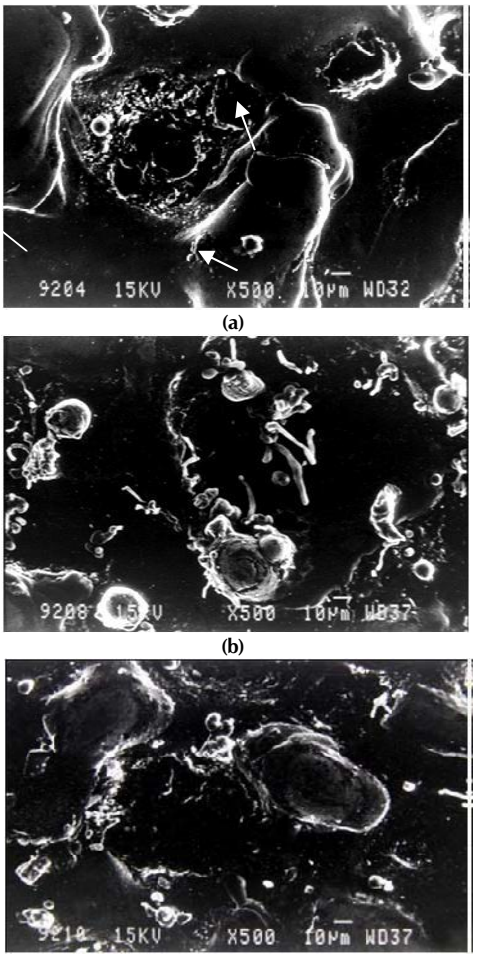

Fig. 5: Appearance of Edmed Surfaces of (A) ADI 1, (B) ADI 2, (C) ADI 3 (Current, 8amp.), Pulse-on (45µs) and Pulse-Off (7µs)

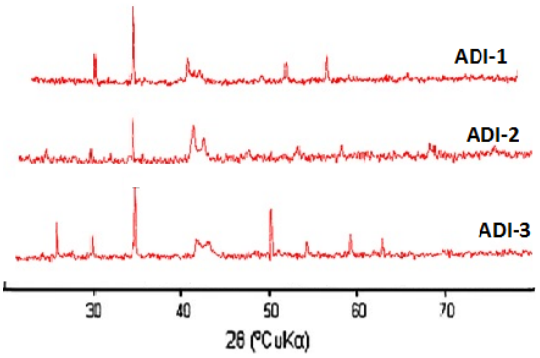

Fig. 6: X-ray Diffraction Pattern of EDMed Surface of ADI-1, ADI-2 and ADI-3

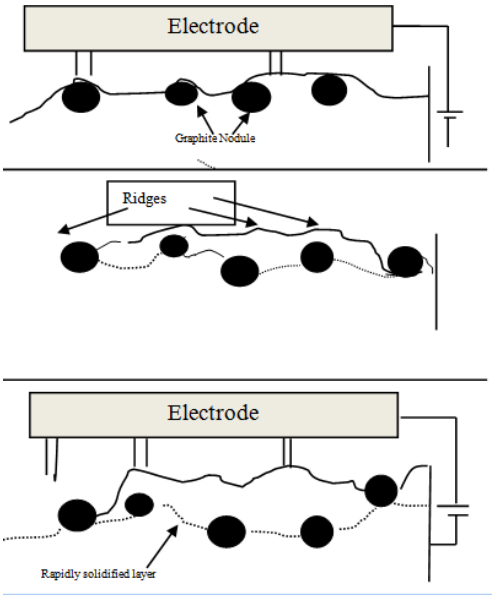

Fig. 7: Schematic Illustration of EDM of ADI

As described in the results, an increase in austempering temperature has nominal effect on EDMed surface roughness and resolidified larger thickness. As explained earlier that the ridge density increases with increase in graphite particle density and decrease in graphite particle size. Thus high nodule count in original DI will increase the surface roughness of EDMed surface as it will lead to numerous discharging points i.e discharge density and thus increase the ridge density and consequently the thickness of the resolidified layer is increased.

Previous studies have reported the structure of EDMed surface layers in ferrous alloys [11, 12]. The structural difference of the recast layer between ADI and other ferrous alloy can be recognized as resulting from the effect of C and Si contents.

CONCLUSION

1. $A_3B_3C_3$ is the desirable combination of levels of three input process parameters (current, pulse on time and pulse off time) to achieve minimum surface roughness (R_a = 2.09, 2.223, and 2.021 µm for ADI-1, ADI-2 and ADI-3 respectively) and maximum material removal rate (0.36, 0.29 and 0.37 gm/min. for ADI-1, ADI-2 and ADI-3 respectively).
2. The morphology of EDMed surface consisted of a wavy ridge pattern formed by overlapping craters with graphite particles in-between the ridges. The ridge density and resolidified layer thickness is closely related to graphite distribution.
3. A modified surface layer with hardness slightly higher than of ADI is obtained as ADI using EDM method.
4. The resolidified layer comprised mainly of austenite, martensite and carbides. The electrode material did not transfer to resolidified layer.

REFERENCES

[1] Alan P. Druschitz and David C. Fitzgeral (2003), "MADI: Introduction a new, Machineable Austempered Ductile Iron", SAE World Congress, Detroit, Michigan.
[2] Keough R.(1998),"Ductile iron data for design engineers".
[3] Pashby I. R., Wallbank J. (1993), "Ceramic Tool Wear when Machining of Austempered Ductile Iron" Wear, Vol. 162-164, No.1, pp 22-33.
[4] Goldberg M, Smith G T, Berry J T, Littlefair G.(1999), "Machinability assessment and surface integrity characteristics of austempered ductile iron (ADI) using ultra-hard cutting tools". 3rd International Machining and Grinding Conference, Cincinnati, Ohio, USA
[5] Cakir, M. Cemal, Bayram, Ali, Isik, Yahya, Salar, Baris (2005), "The effects of austempering temperature and time onto the machinability of austempered ductile iron. Materials Science and Engineering", Vol.407, No.1-2, pp 147-153.
[6] Seker, Ulvi, Hsirci, Hasan (2006), "Evaluation of machinability of austempered ductile irons in terms of cutting forces and surface quality", Journal of Materials Processing Technology, Vol. 173, No.3, pp 260-268.
[7] Katuku. K., Koursaris. A., Sigalas. I.(2009), "Wear, cutting forces and chip characteristics when dry turning ASTM Grade 2 austempered ductile iron with PcBN cutting tools under finishing conditions", Journal of Materials Processing Technology, Vol. 209, No.5, pp 2412-2420.
[8] Zhang H. T., Li H., Dong H., Man L. (2008), "Cutting Properties in Cutting Austempered Ductile Iron by PCBN Compact Tools in Chinese", Materials for Mechanical Engineering, Vol. 32, No. 8, pp 43-46
[9] Tsai D. C., Lui T. S. and Chen L. H.(2000), Materials Transaction, Vol. 41, pp303-309.
[10] Tsai D. C., Lui T. S. and Chen L. H (1999), AFS Transaction, Vol. 10, pp 389-396.
[11] Lloyd H. K. and Warren R. H. (1965), Journal of Iron Steel Institute, Vol.203, pp 238-247.
[12] Minemura T., Inoue A, Kojiwa, Y and Masumoto T. (1981) Proceedings 5th International Conference on Rapidly Quenched Metals, Sendai, Japan, ed. By T. Masumoto and K Suzuki (The Japan Inst. Of metals 1982) pp1501-1504.
[13] Merdon M. A. E-R. and Arnel R. D. (1989), Surface Engineering, Vol.5, pp158-164.
[14] Mills K.D. (1972), "Spheroidal Graphite Cast Irons: Its Development and Future," Br. Foundryman, Vol. 65, pp 34.
[15] Cullity B.D. (1956), Elements of X-ray Diffraction, Addison Wesley Publishing Company, pp 390-396.
[16] Rouns T.N., Rundman K. B., and Moore D. J. (1984), "On the Structure and Mechanical Properties of ADI, " AFS Transaction Vol.,92, pp815-40.
[17] Darwish N., and Elliot R.(1993), "Austempering of Low Manganese Ductile Iron, Part 3. Variation of Mechanical Properties with Heat-Treatment Conditions," Materials Science and Technology, Vol. 9, pp 882-89.
[18] Batra U., Ray S., and Prabhakar S. R. (2003), "Austempering and Austempered Ductile Iron Microstructure in Copper Alloyed Ductile iron," Journal of Materials Engg. and Performance, Vol. 112, pp 426-429.

[19] Rundman K.B., Parolini J.R., Moore D.J. (2005), "Relationship Between Tensile Properties and Matrix Microstructure in Austempered Gray Iron," AFS Transactions, Vol. 145(5) pp. 1-15.
[20] Batra U., "Development and Study of Austempered Ductile Iron" Ph.D Thesis, Panjab University, Chandigarh, India, 2001.
[21] Moore D. J., Rouns T. N., and Rundman K. B. (1987), "The Relationship between Microstructure and Tensile Properties in Austempered Ductile Iron," AFS Transaction, Vol. 95, pp 765-74.
[22] Moore D. J., Rouns T. N. and Rundman K. B. (1985), "Structure and Mechanical Properties of Austempered Ductile Iron," AFS Transaction, Vol. 93, pp705-18.
[23] Krishan Raj D., Narasimhan H. N. L., and Seshan S. (1992), "Structure and Properties of Austempered Ductile Iron as Affected by Low Alloy Additions," AFS Transaction, Vol. 100, pp 105-112.
[24] Yan M., and Zhu W. Z. (1996), "Morphology of Banitic Platelets of Austempered Ductile Iron and Their Effects on Mechanical Properties," Journal of Materials Science Letters, Vol. 15(12), pp 1044-1047.
[25] Daber S., Ravishankar K. S., and Rao P. P.(2008), "Influence of Austenitising Temperature on the Formation of Strain Induced Martensite in Austempered Ductile Iron," Journal of Materials Science, Vol. 43(14), pp 4929-4937.
[26] S Daber S. and Rao P. P.(2008), "Formation of Strain-Induced Martensite in Austempered Ductile Iron," Journal of Materials Science, Vol. 43(1), pp 357-367.
[27] Lim L. C., Lee L. C., Wong Y. S. and Lu H. H.(1991) Materials Science and Technology Vol. 7 pp 239-248.
[28] Greene J. E. and Guerrero-Alvarez J. L.(1997), Metallurgical Transaction Vol.5, pp695-706.
[29] Wu C. and Phalke R. D. (1997), AFS Transaction Vol. 105, pp 739-744.